Electronic Supplementary Material (ESI) for ChemComm.

Supporting Information

P-Modified and Carbon-Shell Coated Co Nanoparticles for Efficient Alkaline Oxygen Reduction Catalysis

Jaeyune Ryu,[1] Namgee Jung,[1] Dong-Hee Lim,[2] Dong Yun Shin,[1] Sae Hume Park,[1] Hyung Chul Ham,[1] Jong Hyun Jang,[1]Hyoung-Juhn Kim,[1] and Sung Jong Yoo[1,*]

[1] *Fuel Cell Research Center, Korea Institute of Science and Technology (KIST)*
[2] *Department of Environmental Engineering, Chungbuk National University*

E-mail: ysj@kist.re.kr

I. Synthetic Procedures

I-1. Preparation of C@Co/C and C@Co-P/C

To a solution of carbon black (Vulcan XC-72, 0.1 g) in oleylamine (70 %, Aldrich, 1 mL) and 1,2-octadecene (90 %, Aldrich, 100 mL), which was ultrasonificated for 0.5 h in advance, was added fast a preheated solution (120 ℃, ~1 hr) of cobalt acetylacetonate (97 %, Aldrich, 0.112 g) in trioctylphosphine (90 %, Aldrich; **4mL for C@Co/C** and **10mL for C@Co-P/C**) and oleylamine (70%, Aldrich, 1 mL) at 120 ℃. The reaction mixture was heated up to 300 ℃ and stirred for 2 h with reflux under argon flow. After cooling down, the catalyst solution was washed by filtration with excessive ethanol (1L x 3), and dried under reduced pressure. Then, the as-prepared catalyst was subsequently annealed in argon atmosphere. The annealing temperature was elevated from 20 to 360 ˚C for 30 min, and then was kept at 360 ˚C for 1 h. After that, the temperature was slowly cooled to room temperature in the furnace.

I-2. Preparation of CoO/C

To a solution of cobalt perchlorate hexahydrate (Aldrich, 0.26 g) in 1-octaonl (>99 %, Aldrich, 15 mL), was added fast oleylamine (70%, Aldrich, 0.5 mL) and triply distilled water (1 mL) at 60 ℃. Then, the as-resultant mixture was added to an ultrasonificated suspension of carbon black (Vulcan XC-72, 0.167 g) in 1-octanol (>99 %, Aldrich, 45 mL) at 60 ℃. The final reaction mixture was heated up from 60 ℃ to 160 ℃ and stirred for 12 h, eventually yielding cobalt oxide nanoparticles on carbon black support. After cooling down, the catalyst solution was washed by filtration with excessive ethanol (1L x 3), and dried under reduced pressure. Lastly, the as-prepared sample was subsequently annealed in argon atmosphere to give CoO/C. The annealing temperature was elevated from 20 to 360 ˚C for 30 min, and then was kept at 360 ˚C for 1 h. After that, the temperature was slowly cooled to 20 ˚C in the furnace.

II. Physical Analysis

The particle distribution and size of the prepared cobalt based catalysts were investigated by (high resolution) transmission electron microscopy (FEI, TECNAI F30 ST, 300 keV at KBSI Seoul center & FEI, TITAN, 300 keV at KIST). The chemical distribution of the present cobalt based nanoparticles was examined using scanncing transmission electron microscopy (STEM) and energy dispersive x-ray spectroscopy (EDX) (FEI, TECNAI F30 ST, 300 keV at KBSI Seoul center & FEI, TITAN, 300 keV at KIST). Inductively coupled plasma-atomic emission spectroscopy (ICP-AES) (Thermo, iCAP 6300) was performed to confirm the composition of the prepared materials qauntatively. By X-ray diffraction (XRD) (Rigaku, MiniFlex II) with Cu Kα radiation, the diffraction patterns of catalysts were obtained in 2 theta ranges between 10 and 90˚. X-ray photoelectron spectroscopy (XPS) was measured at the Pohang Accerlarator Laboratory (PAL) using the 8A1 beamline.

Co K edge X-ray absorption spectroscopy (XAS) was recorded at the Pohang Accerlarator Laboratory (PAL) using the 10C beamline (3 GeV; 200 mA top-up mode). The incident beam was monochromatized using a Si (111) double crystal monochromator and detuned by 10 % to minimize the contamination from higher harmonics, in particular, the third order reflection of the silicon crystals. The spectra for K-edge of Co (E_0 = 7709 eV) were taken in a transmission mode with separate He-filled IC Spec ionization chambers for incident and transmitted beams, respectively. Before measuring samples, energy was calibrated by using of Co foil. The energy scan was performed in five regions for good energy resolution in a steep absorption and measurement of X-ray absorption near-edge structure spectroscopy (XANES) spectra at a time, 5 eV-step in region of 7509-7689 eV, 1 eV-step in 7689-7699 eV, 0.25 eV-step in 7699-7739 eV, 0.03 *k*-step in 7739-8249 eV, and 0.04 *k*-step in 8249-8709 eV. Pre-edge absorption due to the background and detector were subtracted using a linear fit to the data in the range of -200 to -60 eV relative to E_0. E_0 was defined as the first inflection point on the rising absorption edge. Each spectrum was then normalized by a constant, extrapolated value to E_0 of third-order polynomial fit over absorption at 150-900 eV relative to E_0. The data analysis package used for XANES was the University of Washington's data analysis program. The XANES spectra were first subjected to background removal by fitting the pre-edge data to a Victoreen type formula over the range of 200 to 80 eV below the edge, followed by extrapolation over the energy range of interest and subtraction from the data. After the removal of the background contributions, the spectra were corrected for edge-shifts

using the second derivatives of the inflection points of the data from the reference channel. The procedures used for normalization were the conventional ones. The normalization value was chosen as the absorbance at the inflection point of one extended X-ray absortion fine structure (EXAFS) oscillation. The spectra were thus normalized by dividing each datum point by the normalization value using the ATHENA software. This process included edge determination from the first inflection point in the absorption data, background subtraction using the AUTOBK algorithm, and normalization of the EXAFS modulations. The spectra were converted from E-space, to k-space, and then underwent a phase shift specific to the scattering element and Fourier transformation into R-space using the Hanning-type window, in order to better visualize the spacing and fit to theory. In a Fourier transform of the raw spectral data, each peak appears at the relative spacing of that particular shell from the scattering atom. The EXAFS plots (Figure S11) show the Fourier Transformations of the absorption spectrum obtained for each sample (C@Co/C and C@Co-P/C).

III. Computiational Methodology

Spin-polarized density functional theory calculations were performed using the Vienna ab initio Simulation Package (VASP)[1-4] with the projector-augmented wave (PAW)[5,6] method. Electron exchange-correlation functionals were represented with the generalized gradient approximation (GGA), and the model of Perdew, Burke and Ernzerhof (PBE)[7] was used for the nonlocal corrections. A kinetic energy cutoff of 500 eV was used with a plane-wave basis set. Bulk structures of Co and Co_2P were obtained from experimental data of Vicent and Figlarz[8] and Wyckoff[9], respectively, and were fully optimized by means of cell volume relaxation. The space groups and DFT optimized lattice parameters of bulk Co and Co_2P are P63/mmc (a = 2.498 Å , b = 2.498 Å, c = 4.039 Å, $\alpha = \beta = 90°$, $\gamma = 120°$) and Pbnm (a = 6.589 Å, b = 5.512 Å, c = 3.508 Å, $\alpha = \beta = \gamma = 90°$), respectively. Maximum errors associated with the DFT calculated lattice parameters compared to experimental data are less than 0.7, and 2.4% for Co and Co_2P, respectively.

A rhombus-shaped supercell (5.00 × 5.00 × 20.2 Å) with a vacuum space of 8.0 Å and a tetragonal supercell (6.59 × 5.51 × 22.80 Å) with a vacuum space of 14.0 Å were used for the Co and Co_2P surfaces, respectively, as shown in Figure S12. The Brillouin zone integration of the Co–(2×2) and Co_2P–(1×1) surfaces were carried out using 6 × 6 × 1 and 8 × 8 × 1 Monkhorst-Pack grid[12], respectively, and first-order Methfessel-Paxton smearing[13] with a width of 0.1 eV. All atoms were fully relaxed and optimized until the forces were reduced below 0.02 eV/Å .

The adsorption energy (E_{ads}) of atomic oxygen is defined as $E_{ads} = E_{Surf+O} - E_{Surf} - 1/2E_{O2}$, where E_{Surf+O}, E_{Surf}, and E_{O2} are the total energies of the Co and Co_2P systems with adsorbed O, bare Co and Co_2P surfaces, and a gas phase oxygen molecule. A negative adsorption energy indicates that adsorption is exothermic (stable) with respect to the free gas phase hydrogen. Atomic oxygen adsorption was examined on Co and Co_2P surfaces. Among the examined adsorption sites, the most stable configurations of adsorbed oxygen on both surfaces are where oxygen is adsorbed on a hollow site as shown in Figure S12. Table S2 summarizes the oxygen adsorption energies. As the number of P atom increases, the magnetic moments of Co are lost (quenched) as demonstrated in the magnetization comparison in Table S2.

IV. Electrochemical Measurements

All electrochemical measurements were conducted in a standard three-compartment electrochemical cell using a glassy carbon electrode of the rotating disk electrode (RDE), Pt wire, and saturated calomel electrode (SCE) as a working, counter, and reference electrode, respectively. All measurements were reported versus reversible hydrogen electrode (RHE), and performed at room temperature (~25 ^{o}C) in 0.1 M KOH. The RHE calibration was performed in hydrogen saturated electrolyte with a Pt coated disk electrode as the working electrode. The potential at which the current crossed zero was taken to be the thermodynamic potential for the hydrogen electrode reactions (Potential shifts vs SCE: 1.000 V for 0.1 M KOH).

For the catalyst ink slurry, 5 mg of catalyst (C@Co-P/C) and 41 μL of 5 wt % Nafion solution were dispersed in 600 μL of 2:1 v/v ethanol/isopropanol mixed solvent by sonification to form a homogeneous ink. Then, 10 uL of the catalyst ink was loaded onto a glassy carbon electode (0.196 cm^2, geometric surface area), leading to the catgalyst loading (based on cobalt mass) ~0.08 mg_{Co}/cm^2. The dried electrode was then transferred to the electrochemical cell.

The RDE measurements were conducted to evaluate the ORR activities of Co/C, CoO/C, C@Co/C, C@Co-P/C and 20 wt% Premetek Pt/C (catalyst loadings: ~0.08 mg_{Co}/cm^2 for Co-based materials and ~8 $\mu g_{Pt}/cm^2$ for Pt/C). Before ORR tests, blank CV data were measured with rotating speed of 1600 rpm by 5 mV/s from 0.05 to 1.05 V in Ar-saturated 0.1 M KOH. After O_2 gas was purged for ~30 min, the potential was scanned with rotating speed of 1600 rpm by 5 mV/s from 0.05 to 1.05 V with purging O_2 gas. The ORR curves were corrected by the anodic currents of the blank CV. The accelerated degradation test (ADT) was performed to check the durability of C@Co-P/C. After potential cycling of 5,000 times (scan rate = 0.1 V/s) between 0.45 and 0.95 V in O_2-saturated 0.1 M KOH, ORR test was repeated in O_2-saturated 0.1 M KOH (1600 rpm by 5 mV/s from 0.05 to 1.05 V).

The OER activities of C@Co/C and C@Co-P/C were also evaluated by RDE measurements. After Ar gas was purged for 30 min, the potential was scanned with rotating speed of 1600 rpm by 5 mV/s from 1.00 to 2.00 V with purging Ar gas.

For the RRDE measurement, the catalyst ink was prepared by the identical method as RDE's. 13 uL of the catalyst ink was loaded onto a RRDE electode (Pine Instrument, E7R9 series - disk area: 0.2475 cm^2, ring area: 0.1866 cm^2), to achieve the catalyst loading, ~0.08 mg_{Co}/cm^2. The dried electrode was then transferred to the electrochemical cell. After O_2 gas was purged for 30 min, the potential was scanned with rotating speed of 1600 rpm by 5 mV/s from 0.05 to 1.05 V with purging O_2 gas. The ring potential was constant at 1.5 V vs RHE. The HO_2^- yields and the electron transfer numbers were calculated by the following equations.[14]

$$\% HO_2^- = 200 * (I_r/N)/(I_d+I_r/N)$$

$$n= 4* I_d/(I_d+I_r/N)$$

(I_d = disk current, I_r = ring current, N = current collection efficiency of the Pt ring, 0.37)

V. Supplementry Figures

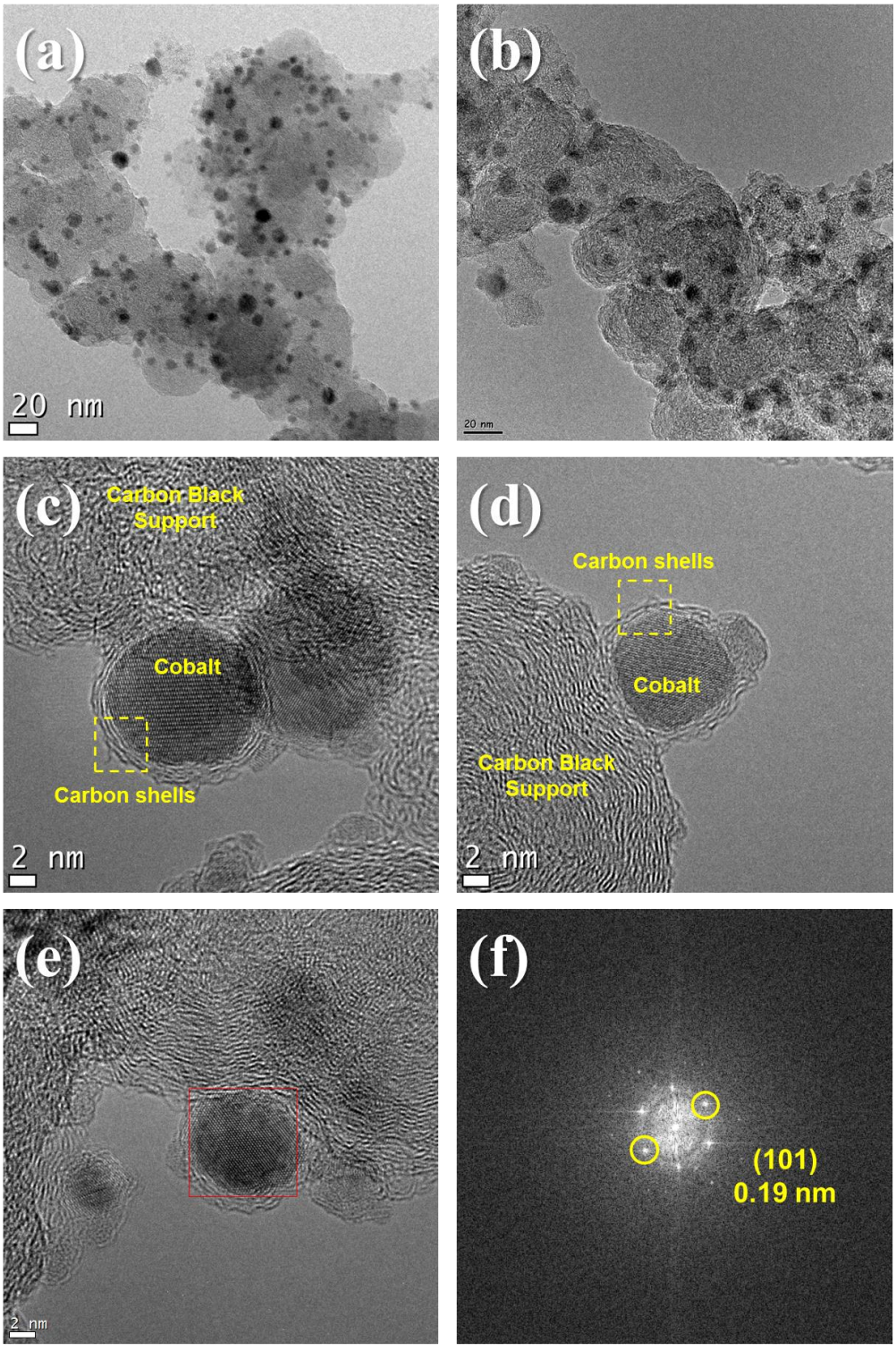

Figure S1. (a-e) TEM images of C@Co-P/C. Average particle size is ~8 nm. (f) Selected area electron diffraction patterns for indicated red box in (e).

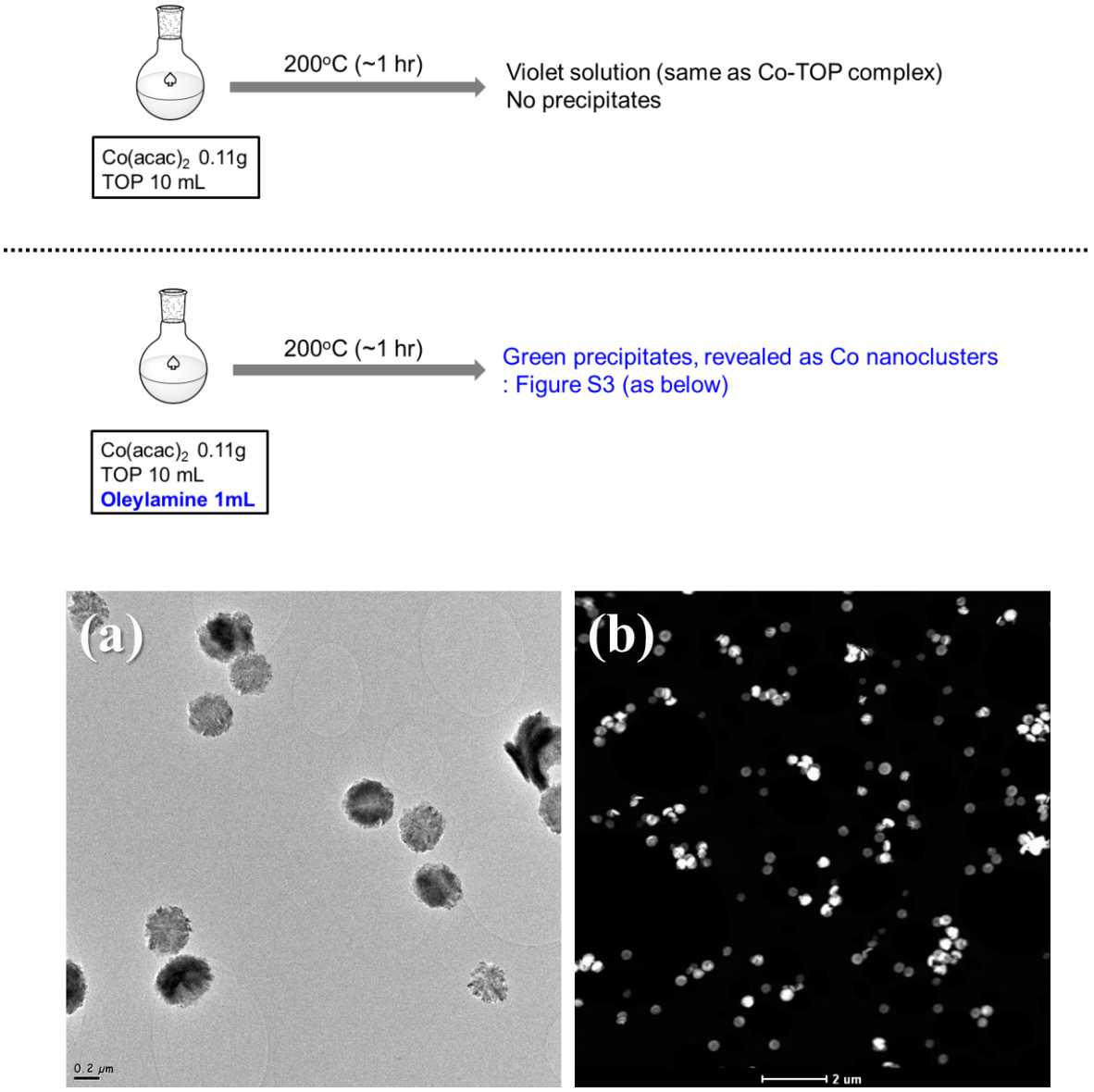

Figure S2. TEM and STEM images of nanoclusters obtained from the reaction with $Co(acac)_2$, TOP, and oleylamine.

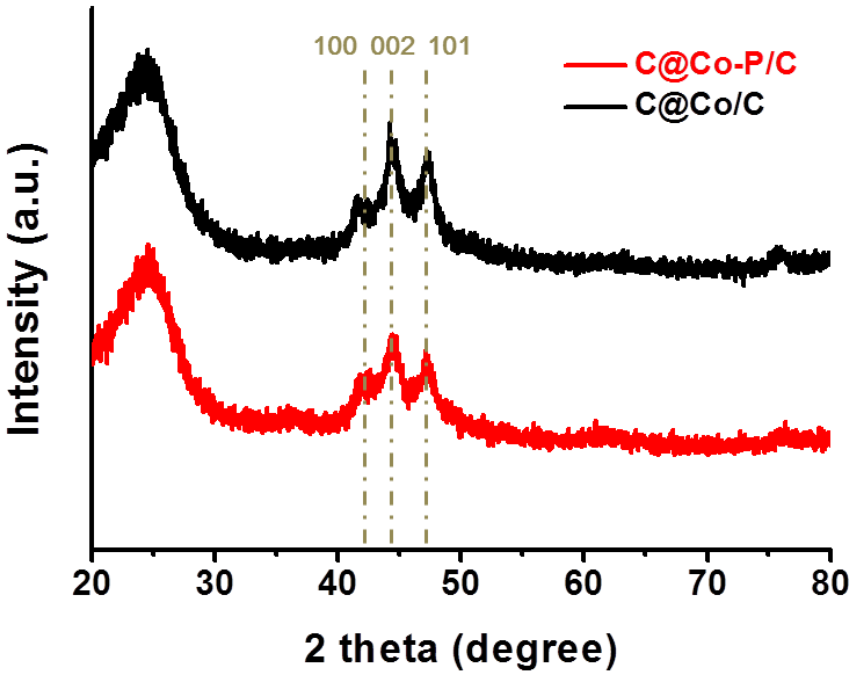

Figure S3. XRD spectra of C@Co/C and C@Co-P/C (hcp Co: JCPDS-05-0727, fcc Co: JCPDS-15-0806).

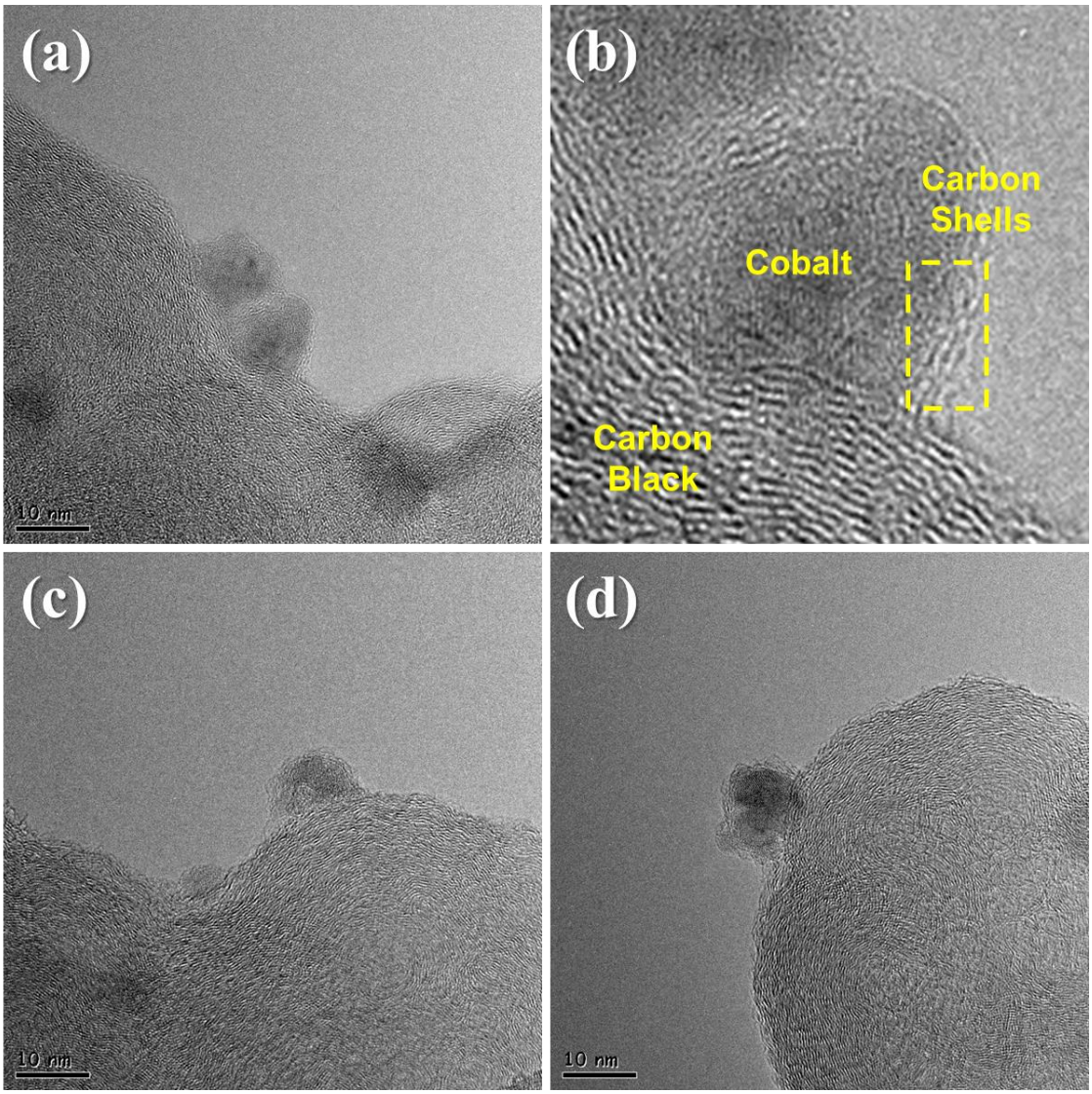

Figure S4. TEM images of as-prepared state of C@Co-P/C prior to heat treatment. Outer carbon shell structures are identifiable. The figure (b) is a further magnified image of figure (a).

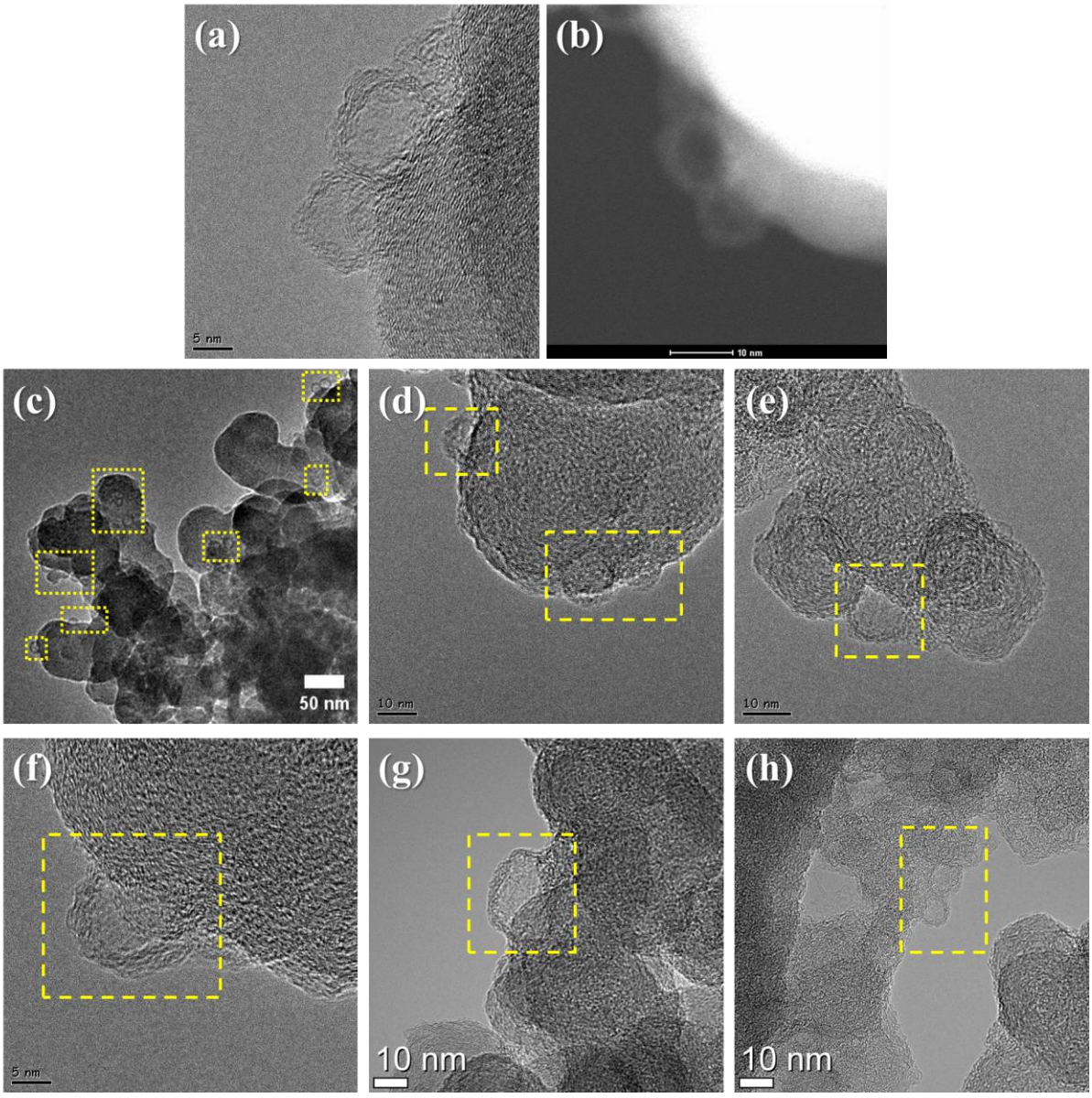

Figure S5. Image dada (TEM and STEM) of hollow carbon shell structures obtained after acid leaching (0.5 M H_2SO_4, 80 ^oC) of C@Co-P/C.

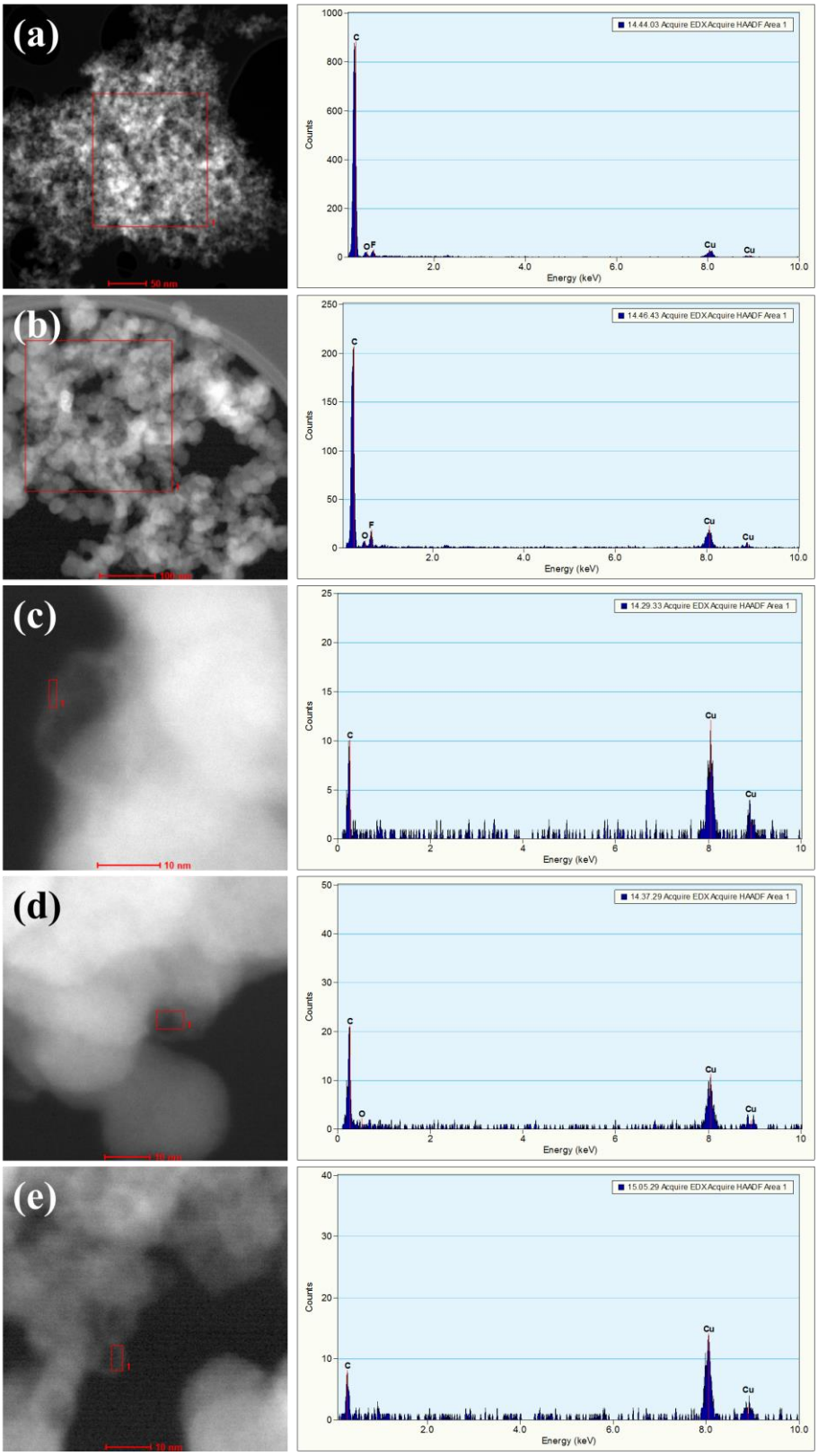

Figure S6. STEM images and EDX analysis of carbon structures obtained after acid treatement (0.5 M H_2SO_4, 80 ^oC) of C@Co-P/C. Non-detectable EDX peak for P indicates low possibility of P-doping into hollow carbon shells and carbon black support.

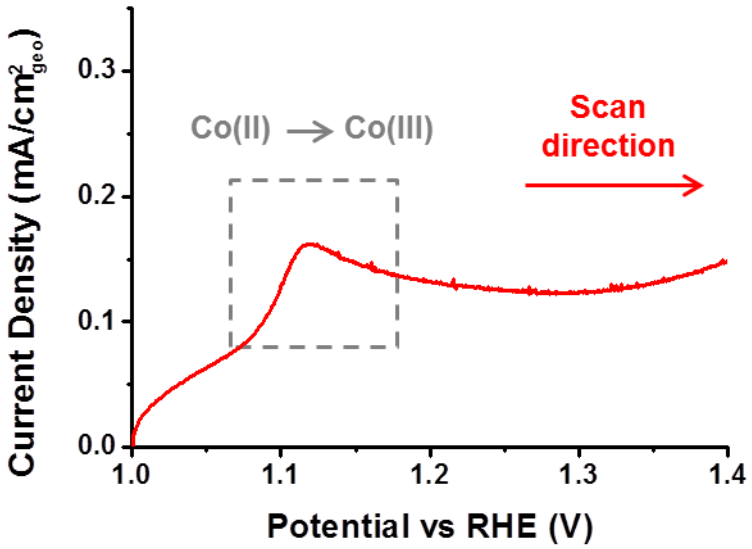

Figure S7. The voltammogram measured by CV method in 0.1M KOH (5mV/s). The oxidation peak of cobalt speices ($Co^{II} \rightarrow Co^{III}$) verifies the redox interaction between cobalt and electrolyte, also indicating the accessibility of electrolyte across the carbon shells to cantact cobalt of C@Co-P/C.

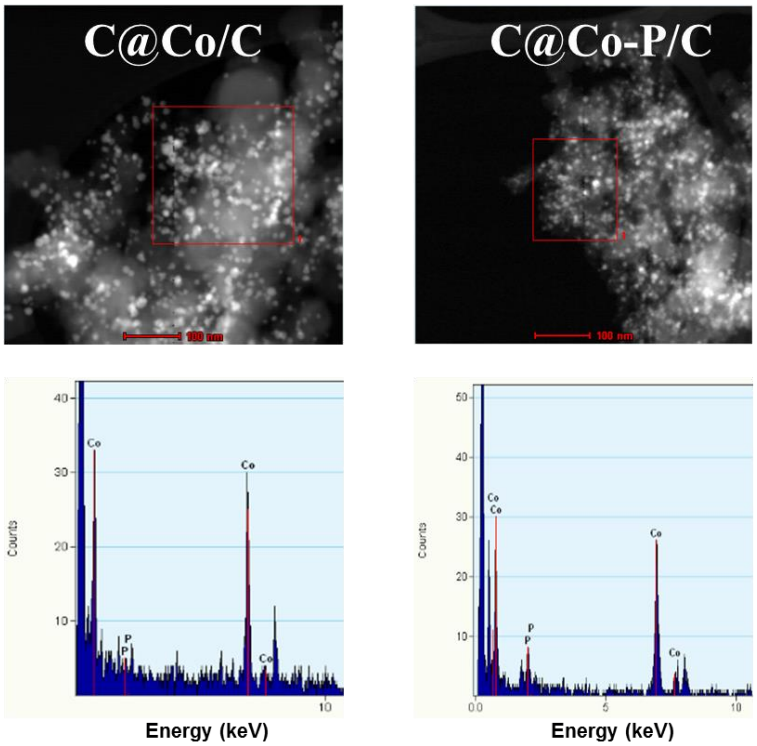

	C@Co/C	C@Co-P/C
Co (at.%)	97.2	78.2
P (at.%)	2.8	21.8

Figure S8. EDX analysis of C@Co/C and C@Co-P/C to estimate the atomic ratio between cobalt and phosphorous.

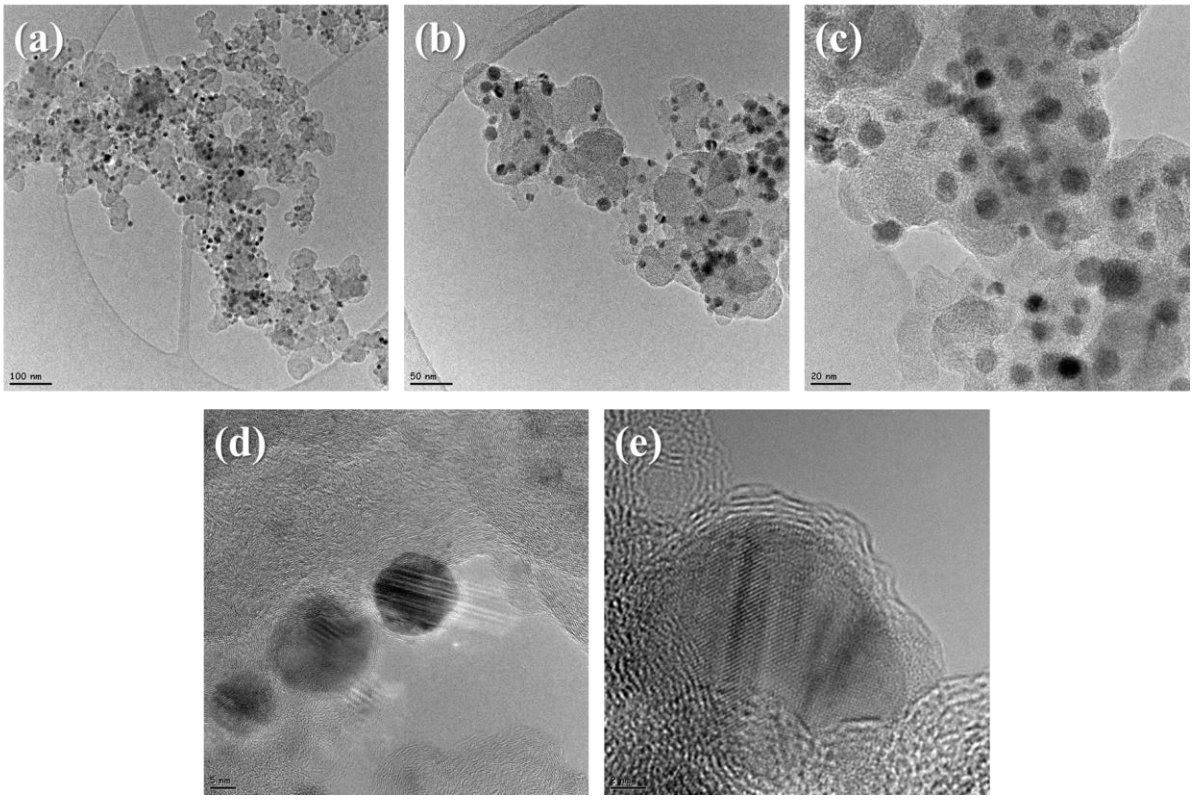

Figure S9. TEM images of C@Co/C. Average particle size is ~10 nm. Similar to C@Co-P/C, outer carbon shell structures are shown in the high resolution images, (d) and (e).

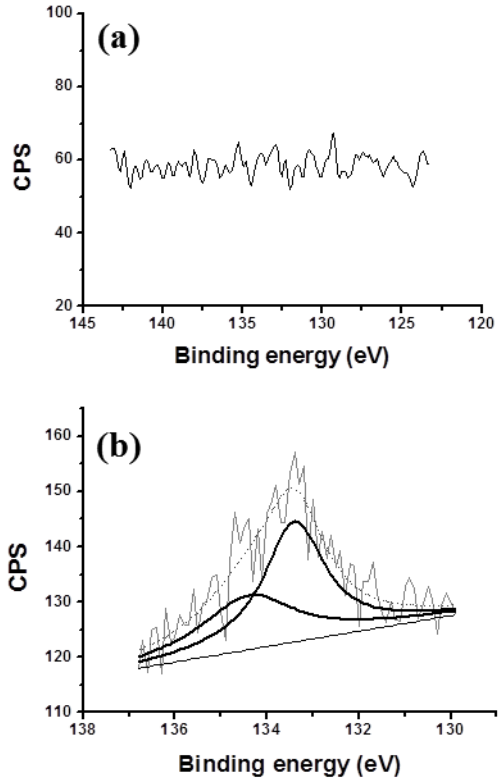

Peak	Position (eV)
0 ($2p_{3/2}$)	133.400
1 ($2p_{1/2}$)	134.400

Figure S10. P 2p XPS spectra of (a) C@Co/C, and (b) C@Co-P/C. For C@Co-P/C, two fiting peaks with ~133 eV and ~134 eV binding energies correspond to the $2P_{3/2}$ and $2P_{1/2}$ core levels of phosphorus, respectively, in phosphate species.[15,16]

Table S1. Co $2p_{3/2}$ XPS fitting results of C@Co/C and C@Co-P /C.[17-19]

Sample	Bond	Position (eV)	Area	FWHM (eV)	Ratio %
C@Co/C	**Peak 0 (Co^0)**	**778.7**	**266.035**	**1.145**	**39.9 %**
	Peak 1 (Co^{II})	782.1	315.482	5.875	47.3 %
	Peak 2 (Sat.)	788.5	84.765	2.130	12.7 %
C@Co-P/C	**Peak 0 (Co^0)**	**779.1**	**144.199**	**1.296**	**10.2 %**
	Peak 1 (Co^{II})	782.5	869.655	3.909	61.8 %
	Peak 2 (Sat.)	787.5	393.347	4.474	28.0 %

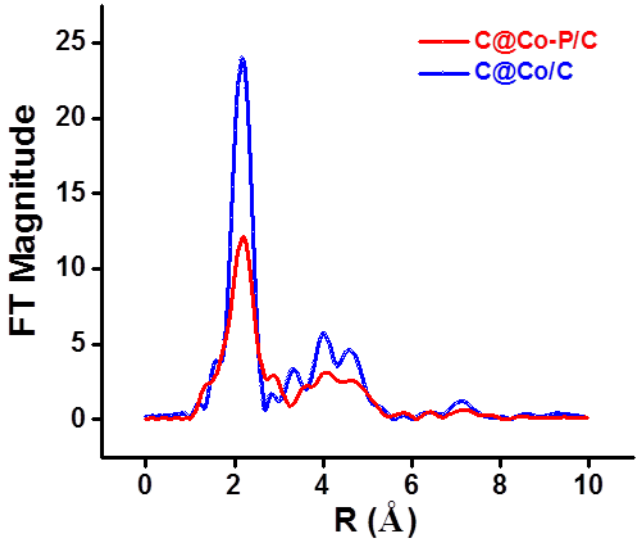

Figure S11. Fourier transformed EXAFS spectra collected at the Co K edge of C@Co-P/C and C@Co-C.

Table S2. *d*-band centers (d_{avg}) of a surface Co atom below the Fermi level, magnetization (total number of spin-up – spin-down electron), and adsorption energies of atomic oxygen on Co_2P, and Co surfaces.

	d_{avg} (eV)	Magnetization (*e*)	Adsorption energy (eV)						
			1	2	3	4	5	6	7
Co_2P	–1.72	6.36	–3.37	–3.37	–3.35	–2.60	–2.55	–2.39	–2.28
Co	–1.93	33.33	–3.24	–3.20	–3.20	–1.72			

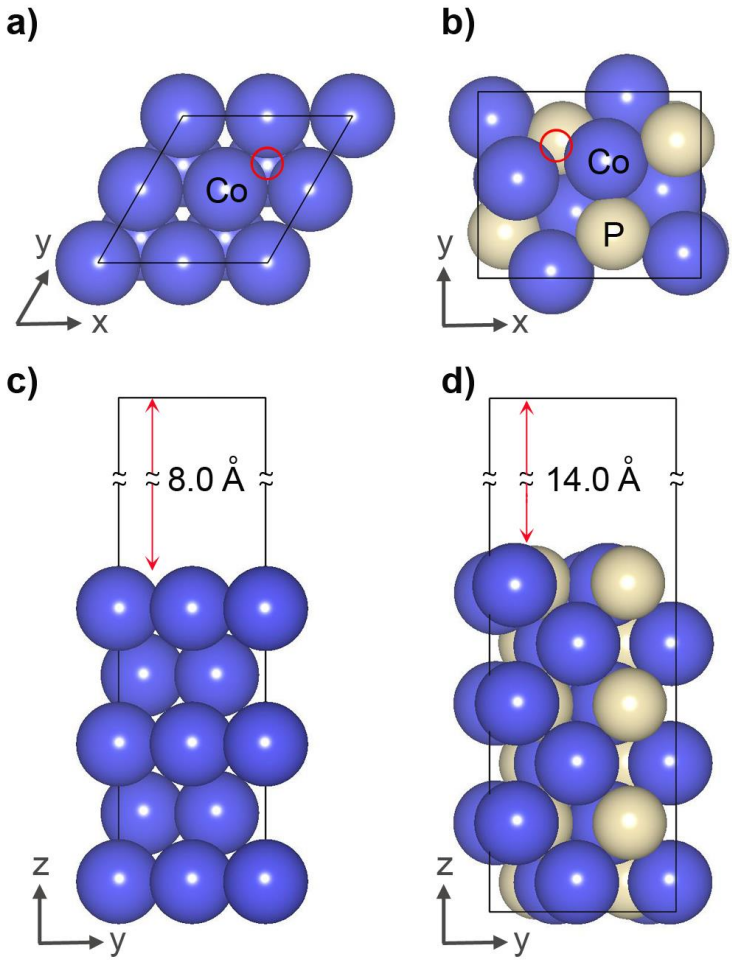

Figure S12. Top and side views of Co and Co_2P surfaces with vacuum space distances. The large (blue) and small (light yellow) spheres represent Co and P, respectively. Red circles indicate the most stable adsorption sites for atomic oxygen. Solid lines indicate the supercells.

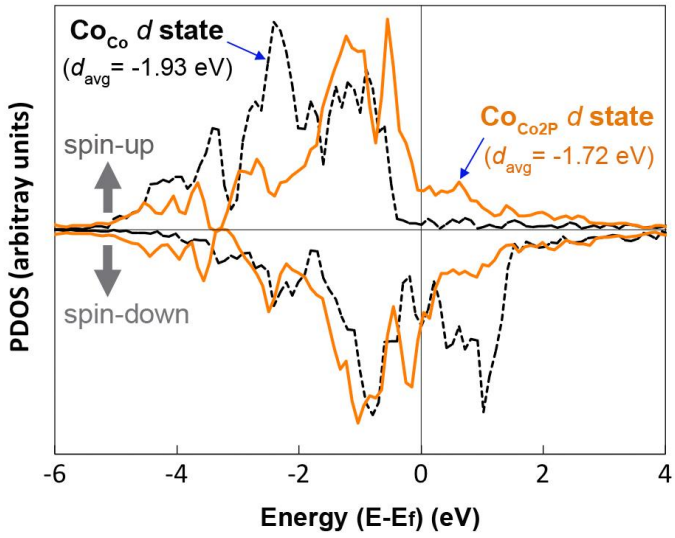

Figure S13. Projected density of states (PDOS) of Co *d* states of Co and Co_2P. Spin-up and -down are indicated by positive and negative values, respectively. The Fermi energy is referenced at 0 eV.

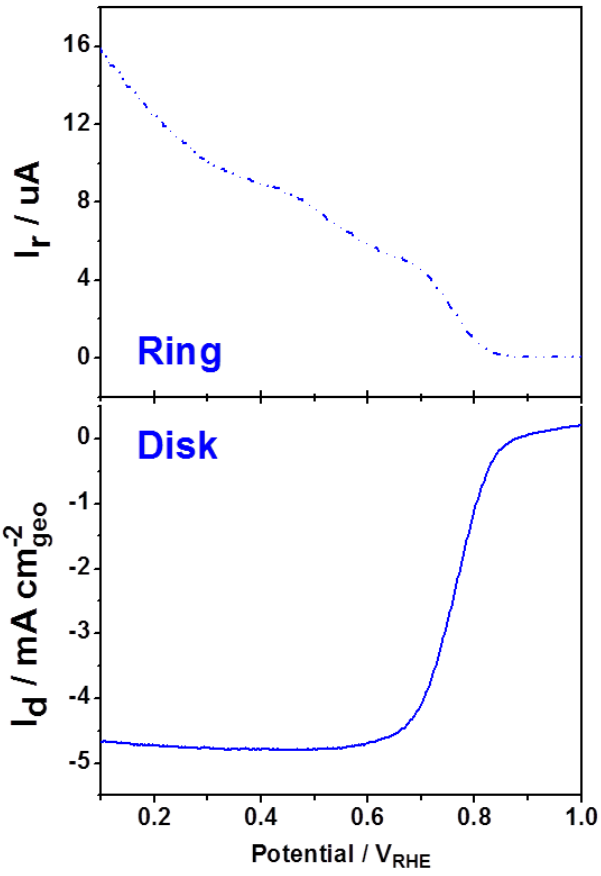

Figure S14. RRDE data (disk and ring currents) of C@Co-P /C (before iR correction) measured in 0.1 M KOH (catalyst loading ~0.08 mg_{Co}/cm^2).

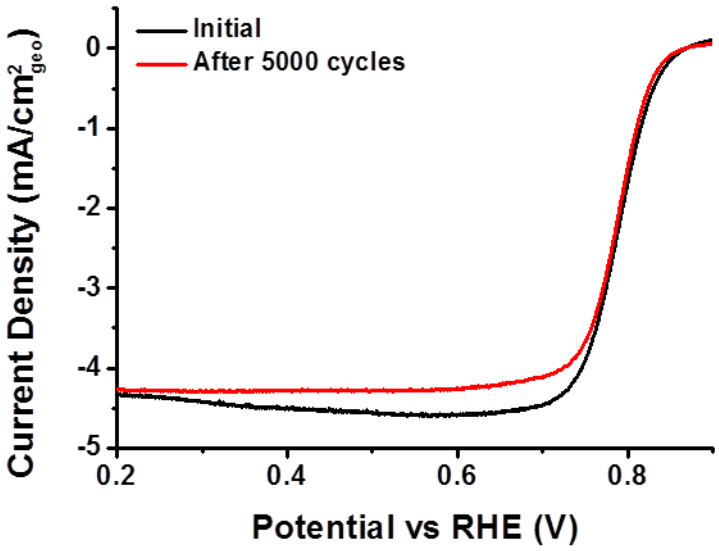

Figure S15. ORR polarization curves of Co@Co-P /C catalyst before and after durability test (0.1M KOH, 5 mV/s, 1600 rpm). 5000 cycles were swept between 0.45 V to 0.95 V at 0.1 V/s under O_2 saturation.

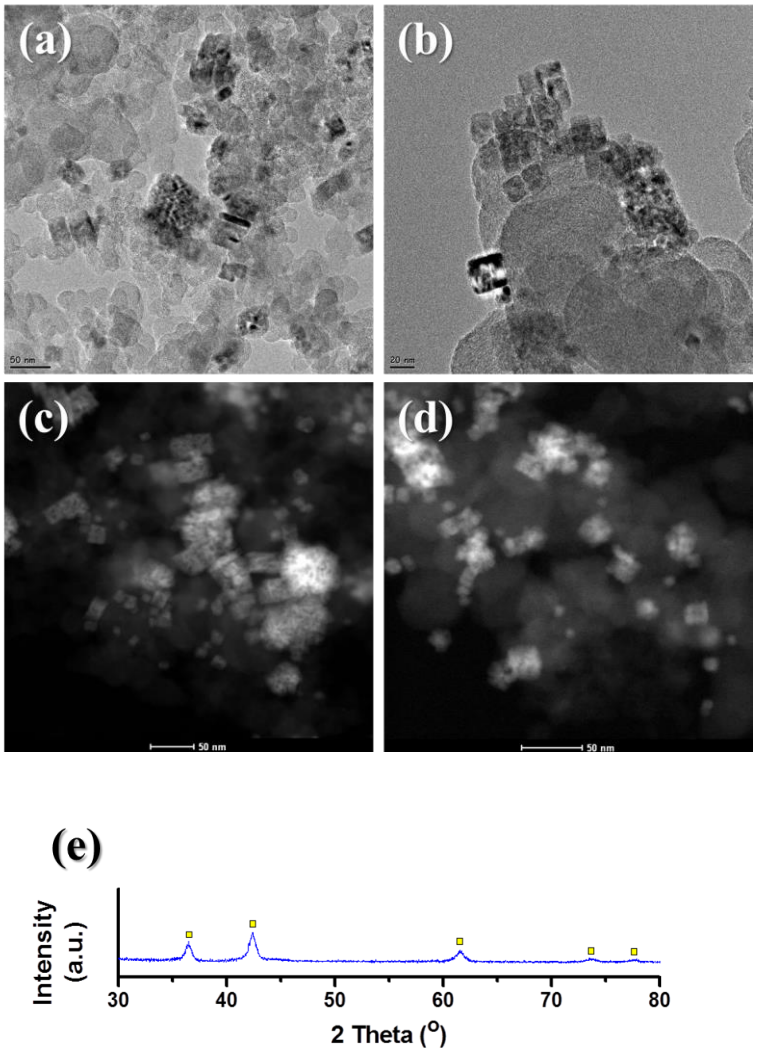

Figure S16. (a-b) TEM and (c-d) STEM images of CoO/C. Average particle size of CoO is 15.5 ± 8.1 nm. (e) XRD data of CoO/C matched with [CoO, JCPDS-43-1004]. Cobalt weight percent in CoO/C is 17 % according to ICP analysis.

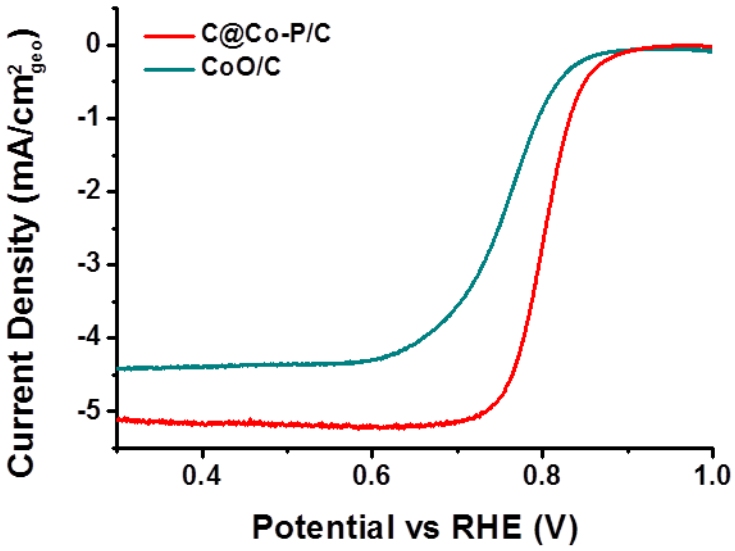

Figure S17. ORR polarization curves of CoO/C (Figure S14) and C@Co-P/C (0.1M KOH, 5 mV/s, 1600 rpm, catalyst loadings: ~0.08 mg_{Co}/cm^2).

VI. References

(1) Kresse, G.; Hafner, J. *Physical Review B* **1993**, *47*, 558.

(2) Kresse, G.; Hafner, J. *Physical Review B* **1994**, *49*, 14251.

(3) Kresse, G.; Furthmüller, J. *Physical Review B* **1996**, *54*, 11169.

(4) Kresse, G.; Furthmüller, J. *Computational Materials Science* **1996**, *6*, 15.

(5) Blöchl, P. E. *Physical Review B* **1994**, *50*, 17953.

(6) Kresse, G.; Joubert, D. *Physical Review B* **1999**, *59*, 1758.

(7) Perdew, J. P.; Burke, K.; Ernzerhof, M. *Physical Review Letters* **1996**, *77*, 3865.

(8) Vincent, F.; Figlarz, M. *C. R. Hebd. Seances Acad. Sci*. **1967**, *264C*, 1270.

(9) Wyckoff, R. W. G. Crystal Structures, 1, **1963**, Second edition. Interscience Publishers, New York, New York.

(10) Rajamani, V.; Prewitt, C. T. *The Canadian Mineralogist* **1974**, *12*, 253.

(11) Parise, J. B. *Acta Crystallographica Section B-Structural Science* **1980**, *36*, 1179.

(12) Monkhorst, H. J.; Pack, J. D. *Physical Review B* **1976**, 13, 5188.

(13) Methfessel, M.; Paxton, A. T. *Physical Review B* **1989**, 40, 3616.

(14) Paulus, U. A.; Schmidt, T. J.; Gasteiger, H. A.; Behm, R. J. *J. Electroanal. Chem.* **2011**, 495, 134.

(15) Hu, G.-R.; Deng, X.-R.; Peng, Z.-D.; Du, K. *Electrochim Acta.* **2008**, *53*, 2567.

(16) Cobo, S.; Heidkamp, J.; Jacques, P.-A.; Fize, J.; Fourmond, V.; Guetaz, L.; Jousselme, B.; Ivanova, V.; Dau, H.; Palacin, S.; Fontecave, M.; Artero, V. *Nat. Mater.* **2012**, *11*, 802.

(17) Korányi, T. I. *Appl. Catal. A* **2003**, *239*, 253.

(18) Grosvenor, A. P.; Wik, S. D.; Cavell, R. G.; Mar, A. *Inorg. Chem*. **2005**, *44*, 8988.

(19) Abu, I. I.; Smith, K. J. *J. Catal.* **2006**, *241*, 356.